Korean J. Chem. Eng., 35(9), 1948-1953 (2018)
DOI: 10.1007/s11814-018-0095-8

pISSN: 0256-1115
eISSN: 1975-7220

Agglomeration characteristics of nano-size TiO_2 particles using analytical solution

Jong-Sang Youn*,‡, SeJoon Park,‡, Hyunwook Cho*, Yong-Won Jung*, and Ki-Joon Jeon*,†**

*Department of Environmental Engineering, Inha University, 100 Inha-ro, Nam-gu, Incheon 22212, Korea
**Department of Industrial and Management Engineering, Myongji University,
Myongji-ro 116, Cheoin-gu, Yongin-si, Gyeonggi-do 17058, Korea
(*Received 22 April 2018 • accepted 4 June 2018*)

Abstract−We developed equations for nano-sized titanium dioxide (TiO_2) particles self preserving time (SPT) lag that combines with agglomerate key parameters such as primary particle size (PPS), geometric standard deviation (GSD) and mass fractal dimension (MFD). A statistical formula has been developed that relies on SPT lag as the key parameter of agglomerates. Finally, this research presents the first analytical solution by integrating these key parameters into one formula, which can be utilized as a handy tool to calculate the time for reaching the asymptotic state.

Keywords: Mass Fractal Dimension, Self Preserving Time, Agglomerate, Nanoparticle, Primary Particle Size, Geometric Standard Deviation

INTRODUCTION

Coagulation is one of the common processes that can be easily found in many advanced materials in diverse industry fields [1-4]. Particles are formed by gas-to-particle conversion under high temperature condition followed by coagulation which is composed of nanoparticle chains agglomerates [1,5]. Many studies have been conducted to figure out the synthesis process and the properties of particles, and many applications of nanoparticles are pouring out [2-4].

Experiments have been attempted to grasp Brownian coagulation with agglomerations. For instance, Matsoukas and Friedlander [6] showed that the rate of coagulation in the production of metal oxide particles increased with decreasing mass primary particle size (PPS) and fractal dimension. One example is that the PPS of commercially available TiO_2 (Degussa AG, TI 1234) agglomerates is between few nm to 20 nm in flame and diffusion reactors [1]. In a recent study, non-spherical titania agglomerates enlarged much faster than spherical agglomerates [7]. Then, non-spherical titania agglomerates moved to an asymptotic mass fractal dimension (MFD) while oxidation proceeded in high temperature [7]. Furthermore, the morphological transition of agglomerates was evaluated using Monte-Carlo simulations in many processes including diffusion [8], sintering and coagulation [9]. One study performed a stochastic simulation algorithm wherein the primary particle was observed in order to find its movement and determine the role of deterministic and stochastic forces on the particle [10]. Another study provided simulation results of agglomeration using computational algorithm [11]. Morphology of agglomerates was classified as reaction-limited and diffusion-limited with the proposed mechanism [12].

Aerosol dynamics models are another ones developed in order to figure out how the morphological structure affects the behavior of aerosol agglomerates. A variety of aerosol models are accessible to explain aerosol dynamics on the basis of mathematical delineation of particle size distribution, such as moment [13-15] and sectional models [16,17]. The evolving agglomerates were simulated starting from individual spherical particles, which assumed power law distribution and evaluated the influences of fractal dimension and PPS [18]. Self-preserving time (SPT) lag was provided by Vemury et al. [19] to calculate the time to reach the asymptotic size distribution. A correlation equation of the two was devised for SPT in the free molecular as well as continuum regimes in terms of initial geometric standard deviation (GSD). The simulations were conducted with a discrete sectional model. In a later study, MFD was integrated into the model and its effects were investigated [20].

The first analytical solution was proposed in order to trace the evolving size distribution of spherical aerosols regarding lognormal distribution and undergoing Brownian coagulation in the free molecular regime [21]. The analytical solution was extended later to include fractal agglomerates with a focus on changes of the SPT lag as a function of MFD. In addition, the sectional model [17] and analytical solution [22] were compared to predict the shape of the asymptotic agglomerate size distribution. The sectional method was used to calculate the asymptotic values of 1.46, 1.52, and 1.61 for D_f of 3.0, 2.5, and 2.0, respectively. In contrast, Park and Lee [22] obtained the asymptotic values by analytical solutions, resulting in 1.36, 1.39, and 1.48, respectively. However, what was overlooked in both studies is that they did not address the effect of PPS. It has been identified that the size of primary particles is an important variable from previous experimental studies. Ulrich and Subramanian [23] also emphasize the importance of PPS by describing the physical properties and behavior of agglomerates generated from the gas phase at high temperature. The properties immensely rely on

†To whom correspondence should be addressed.
E-mail: kjjeon@inha.ac.kr
‡Both authors contributed equally to this work.

the agglomerate size and the number and size of primary particles.

The time to reach asymptotic distribution has much to do with nanoparticle synthesis as noted in previous studies. Thus, the aim of this study was to develop equations for nano-sized TiO_2 particles SPT lag incorporating all important parameters of agglomerates such as PPS, GSD, and fractal dimension. We especially focused on the effect of primary particle diameter (PPD), which has been shown to influence coagulation rate. Moreover, we demonstrated the effectiveness of the other two parameters on PPS.

METHOD

1. Model Development

Eq. (1) describes the particle size distribution by Brownian coagulation using an integro-differential equation.

$$\frac{\partial n(v_j, t)}{\partial t} = \frac{1}{2}\int_0^{v_j} \beta(v_i, v_j - v_i) \times n(v_i, t) \times n(v_j - v_i, t) dv_i - n(v_j, t)\int_0^{\infty} \beta(v_i, v_j) \times n(v_i, t) dv_i \quad (1)$$

where $n(v_j, t)$ refers the particle size distribution as a function of time t and the two particles collision kernel which is for two particles having volume v_i and v_j, respectively [24]. The collision kernel in the regime of free molecular is expressed in Eq. (2).

$$\beta(v_i, v_j) = \pi(d_{ai} + d_{aj})^2 \left(\frac{K_b T}{2\pi\rho}\right)^{\frac{1}{2}} \left(\frac{1}{v_i} + \frac{1}{v_j}\right)^{\frac{1}{2}} \quad (2)$$

where $\pi(d_{ai}+d_{aj})^2$ refers the agglomerates of collision cross section and $\left(\frac{K_b T}{2\pi\rho}\right)^{\frac{1}{2}} \left(\frac{1}{v_i} + \frac{1}{v_j}\right)^{\frac{1}{2}}$ refers the average relative velocity between colliding agglomerates. Eq. (3) expresses the number of primary particles in the agglomerate N_{pp} expressed by the relationship between PPD (d_p) and the radius of gyration of the agglomerate (R_g).

$$N_{pp} = \frac{v}{v_0} = k\left(\frac{2R_g}{d_p}\right)^{D_f} \quad (3)$$

where ν_0 refers the primary particle volume, k refers the structure prefactor, and D_f refers the fractal aggregate with a fractal dimension [18,25].

If D_f is between 2 and 3, the agglomerate cross sections can be expressed by

$$\text{cross section} \propto (R_{gi} + R_{gj})^2 \quad (4)$$

The cross section of the new agglomerate without the limitation of D_f may have a result greater than sum of the individual agglomerates' counterparts. Hence, D_f larger than was recommended. Furthermore, the assumption of computer simulation provided D_f is a constant value [24]. k is assigned to 1 in the incorporation of Eqs. (2) and (3). The collision kernel of agglomerates is described in Eq. (5). The kinetic gas theory for rigid spherical particles with D_f larger than 2 in the free molecular regime is described as

$$\beta(v_i, v_j) = K\left(\frac{1}{v_i} + \frac{1}{v_j}\right)^{\frac{1}{2}} \left(v_i^{\frac{1}{D_f}} + v_j^{\frac{1}{D_f}}\right)^2 \quad (5)$$

where, $K = \left(\frac{6k_b T}{\rho}\right)^{\frac{1}{2}} \left(\frac{3}{4\pi}\right)^{\frac{2}{D} - \frac{1}{2}} \left(\frac{d_p}{2}\right)^{2 - \frac{6}{D_f}}$, k_b refers to the Boltzmann constant, ρ means the particle density, and T is the absolute temperature [6].

The coagulation phenomena have been explained by the moment method because of the efficient structure and low computational [26,27]. Eq. (6) explains the particle size distribution at the k^{th} moment.

$$M_k = \int_0^{\infty} \nu^k \cdot n(\nu, t) d\nu \quad (6)$$

In this research, we assumed that the moment model is lognormal size distribution. The function of lognormal size distribution is provided as

$$n(\nu, t) = \frac{1}{3\nu} \frac{N(t)}{\sqrt{2\pi} \ln \sigma_g(t)} \exp\left[\frac{-\ln^2(\nu/\nu_g(t))}{18\ln^2 \sigma_g(t)}\right] \quad (7)$$

where $\sigma_g(t)$ refers the GSD, N(t) refers the total number concentration, and $\nu_g(t)$ refers the geometric number mean volume of particles. Various moment equations can be derived by incorporating Eq. (1) with (6) and (7). The specific details of the moment equation development are provided elsewhere [28]. For the moments, we used the differential equations calculated by a Runge-Kutta 4^{th} order method and for comparison purposes only (Table S1). The key parameters of size distribution including GSD and geometric mean diameter can be decided for each time step. Park and Lee [22] provided various assumptions to derive the analytical solution. Once these equations are numerically solved, the assumptions are no longer needed.

2. Simulation Conditions

We estimated the impact of agglomerate size distribution on coagulation rate by altering PPS, MFD, and initial GSD, which parameters conditions are provided in Table 1. We determined the time to reach the asymptotic state, i.e., SPT lag of fractal agglomerates, τ_f by tracking the development of σ_g. Landgrebe and Pratsinis [17] and Vermury and Pratsinis [19] defined that τ_f is the time takes for σ_g close to the asymptotic value within 1%. The simulation conditions of set 1 were equal to those in prior studies [19, 22], which indicate our results are comparable to results in prior studies. d_p and σ_{g0} in sets 2 and 3 were varied to evaluate the dependence of τ_f.

RESULTS AND DISCUSSION

1. Effects of d_p and D_f to Coagulation Rate

The effects of d_p and D_f to the growth of agglomerates were evalu-

Table 1. Simulation conditions

Set	σ_0	MFD	Particle number concentration (# cm^{-3})	PPS (nm)
1	1			2
2	1	2.0/2.5/3.0	10^{16}	1-20
3	1-3			1-20

ated before performing the simulation. It was carried out by investigating the relationship between spherical particles (β_s) and the collision kernels of agglomerates (β_a) in the same particle volume. In contrast to non-spherical particle β_a in Eq. (5), the spherical particles β_s is expressed in Eq. (8) by setting $D_f=3$.

$$\beta_s=\left(\frac{6k_bT}{\rho}\right)^{\frac{1}{2}}\left(\frac{3}{4\pi}\right)^{\frac{1}{6}}\left(\frac{1}{u}+\frac{1}{v}\right)^{\frac{1}{2}}\left(u^{\frac{1}{3}}+v^{\frac{1}{3}}\right)^2 \tag{8}$$

Dividing Eq. (5) by Eq. (8), the ratio can be derived as

$$\frac{\beta_a}{\beta_s}=\left(\frac{3}{4\pi}\right)^{\frac{2}{D_f}-\frac{2}{3}}\left(\frac{d_p}{2}\right)^{2-\frac{6}{D_f}}\frac{(v^{1/D_f}+u^{1/D_f})^2}{(v^{1/3}+u^{1/3})^2} \tag{9}$$

The ratio of the collision kernels is described in Eq. (10). We assume monodisperse (u=ν) and extreme size ratio (ν>>u).

$$\frac{\beta_a}{\beta_s}=\left(\frac{3}{4\pi}\right)^{\left(\frac{2}{D_f}-\frac{2}{3}\right)}\left(\frac{d_p}{2}\right)^{2-6/D_f}\nu^{\frac{2}{D_f}-\frac{2}{3}}=\left(\frac{2R_g}{d_p}\right)^{\left(2-\frac{2}{3}D_f\right)} \tag{10}$$

where $v=\left(\frac{2R_g}{d_p}\right)^{D_f}\left(\frac{\pi}{6}d_p^3\right)$ following Eq. (3) where k is set to 1. As shown in Eq. (10), higher collision rates were achieved from agglomerates with a smaller PPS and a smaller MFD.

2. Effect of D_f to the Asymptotic GSD (σ_g)

Several researchers reported that σ_g applies to asymptotic value if coagulation is the main mechanism [18,20,22]. We used the analytical calculation provided by Park and Lee [22] to evaluate the asymptotic σ_g (Fig. 1). The fractal agglomerates are almost the same as the analytical results (symbols overlapped) reported by previous research [22]. The self-preserved GSD for D_f=3.0, 2.5 and 2.0 was 1.36, 1.40 and 1.48 respectively. The influences of assumptions used in the previous study [22] are insignificant by confirming the similarity. Similar results were published using the discrete-sectional methods elsewhere [20,18]. Differences between the sectional and moment models result from the presumed size distribution. Thus, those asymptotic values must differ accordingly. Differences between the number and volume based model originate from the finite sectional spacing, which leads to numerical diffusion [17,18].

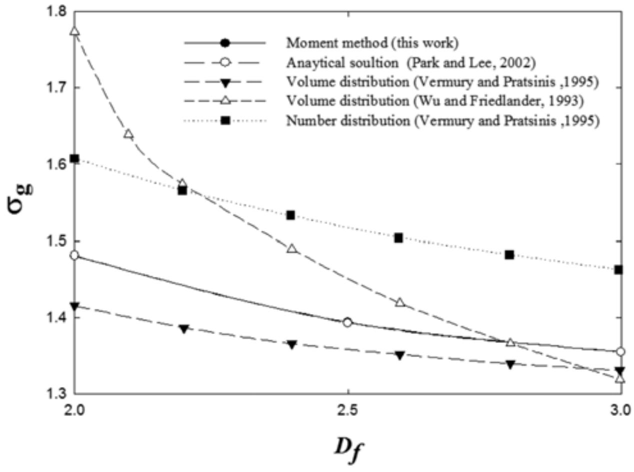

Fig. 1. Asymptotic as a function of D_f [18,20,29].

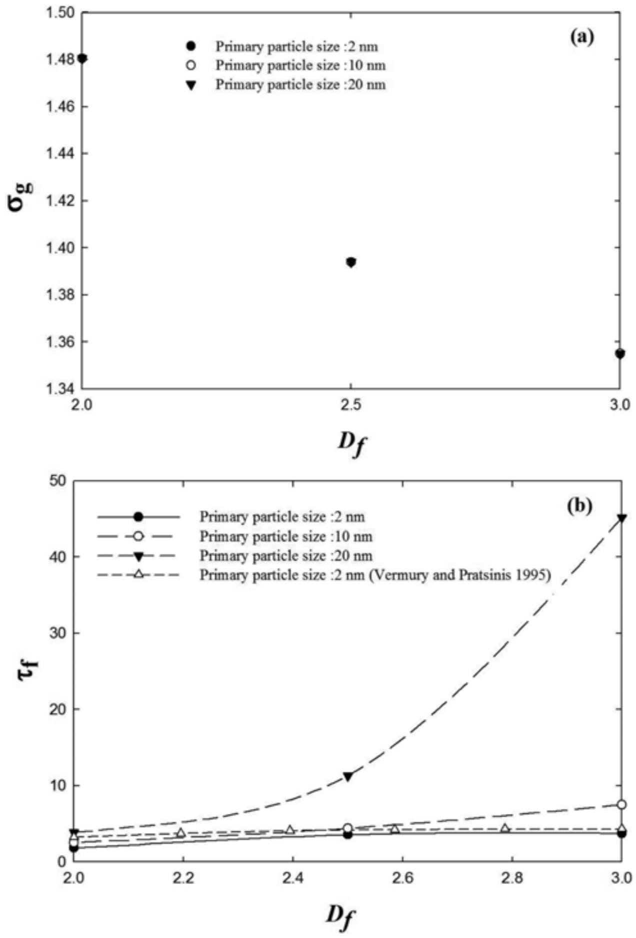

Fig. 2. d_p Effect as a function of D_f on: (a) GSD; (b) SPT lag [20].

3. Effect of d_p to τ_f and σ_g as a Function of D_f

We conducted simulation for d_p to evaluate the influence of d_p on τ_f and σ_g. With all the other parameters remaining constant, we applied 1 nm, 10 nm, and 20 nm of d_p values. σ_g as a function of D_f is shown in Fig. 2(a) for 3 PPS and the effect of d_p is insignificant. On the other hand, d_p has a large effect to τ_f as shown in Fig. 2(b). τ_f was calculated using Eq. (11).

$$\tau_f=\left(\frac{3k_bTd_p}{\rho_p}\right)^{\frac{1}{2}}\left(\frac{3}{4\pi}\right)^{\frac{1}{6}}N_0t \tag{11}$$

where t was obtained by the simulation runs [20].

When d_p=2 nm, τ_f does not change much along different D_f. In addition, they are very similar to those of the sectional method even though σ_g are different [20]. However, the impact on τ_f becomes dominant as d_p and D_f increase. $\tau_{20\,nm}$ is around 15 times larger than $\tau_{2\,nm}$ (D_f=3) despite the same asymptotic σ_g value for both (Fig. 2(a)).

Small primary particles in the agglomerates are likely to have larger drag forces so that their coagulation speed is faster than large particles. Therefore, smaller primary particles can reach the asymptotic value faster. Then, we investigated a statistical formula for τ_f as a function of D_f where the PPS was 2 nm. Eq. (12) shows a one-way non-linear regression model with an exponential relationship:

$$\tau_{2\ \mathrm{nm}} = \frac{1}{0.2734 + \exp\left(\frac{42.1}{D_f^2} - 11.8\right)} \quad (D_f \geq 2.0) \tag{12}$$

We adopted the exponent following the ones by Park et al. [30]. When we compared Eq. (12) to prior research [20], the results between two methods (discrete-sectional and moment) were very similar for d_p=2 nm (Fig. 2(b)).

4. Combined Effect; d_p and D_f on τ_f

We statistically evaluated the dependence of τ_f on both d_p and D_f using nonlinear regression 2-way ANOVA test (α=5%). Normalized SPT lag (τ_n) was used in this study to facilitate the analysis as the ratio of SPT lag of agglomerates consist of any PPS larger than 2 nm with the same D_f of 2 nm (Eq. (13)).

$$\tau_n = \frac{\tau_f}{\tau_{2\ \mathrm{nm}}} \tag{13}$$

Then, Eq. (14) shows the dependence of τ_n on d_p and D_f.

$$\tau_n = 1.079394 + 1.04 \times 10^{-5} e^{(0.268549 d_p + 2.835173 D_f)} \quad (R^2 = 0.994) \tag{14}$$

The real time lag of agglomerates comprised of given d_p and D_f can be obtained by incorporating Eqs. (13) and (14), and it becomes Eq. (15).

$$\tau_f = [1.079394 + 1.04 \times 10^{-5} e^{(0.268549 d_p + 2.835173 D_f)}] \Big/ \left[0.2734 + e^{\left(\frac{42.1}{D_f^2} - 11.8\right)}\right] \tag{15}$$

Fig. 3 shows the SPT lag for diverse D_f as a function of d_p, and it shows that d_p does not seem to have significant effect with a small D_f (e.g. 2). There was no big change in the SPT lag over the entire range of PPS. In contrast, the influence of d_p on τ_n becomes obvious with increases of D_f.

5. Integrated Effect; d_p, D_f, and σ_{g0} on τ_f

We investigated the reliance of τ_f as a function of d_p, σ_{g0} and D_f using sequential statistical method least nonlinear regression 3-way ANOVA test (α=5%). Fig. 4 describes τ_f of 2 nm agglomerates as a function of σ_{g0} using previous studies [19,21] and this study results.

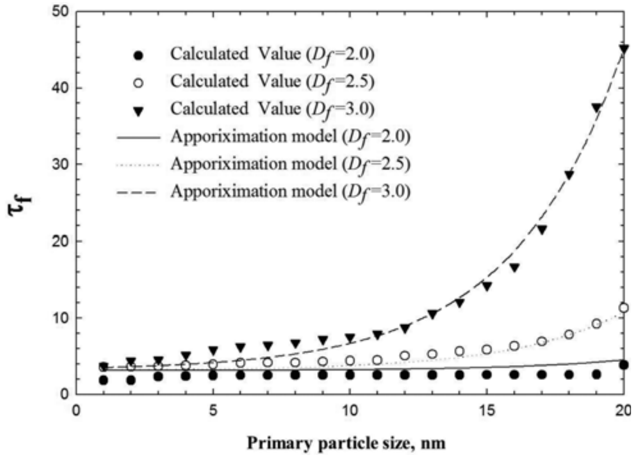

Fig. 3. MFD and PPS effects on τ_f in the free molecular regime.

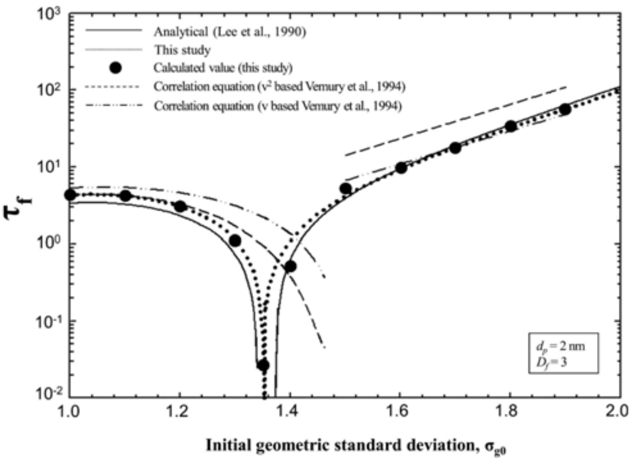

Fig. 4. Comparison of τ_f to obtain the self-preserving distribution [19,21].

To predict τ_f, Vemury et al. [19] applied two correlation equations based on σ_{g0} which was smaller than the asymptotic value,

$$\tau_f = A\sigma_{g0} - B(\sigma_{g0} - 1)^2 \exp[-C(\sigma_{g0} - 1)^3] \tag{16}$$

and for σ_{g0} larger than the asymptotic value,

$$\log_{10} \tau_f = D + E\sigma_{g0} \tag{17}$$

Note that d_p=2 nm and D_f=3 were applied for Eqs. (16) and (17). We statistically obtained that the time lag depends on parameters for the moment model. The format of Eq. (16) was adopted for σ_{g0} smaller than the asymptotic value even though the parameters A-C are not constants anymore. Eq. (18) expresses a new formula for σ_0 larger than the asymptotic value.

$$\tau_f = \exp(D + E\sigma_0) + F (R^2 = 0.992) \tag{18}$$

While variable C is only a function of MFD, it was found that variables A to F in Eqs. (16) and (18) significantly depend on PPS and MFD. We evaluated the dependence of τ_f on all these parameters with 3-way ANOVA test (α=95%). The 3-way ANOVA test includes the A-F factors which are listed in supporting information (SI. 2). The influence of D_f and σ_{g0} on τ_f is described in Fig. 5. As the σ_{g0} approaches to the asymptotic value, the SPT lag becomes shorter. The relationship between σ_{g0} and τ shows an exponential trend. Moreover, it needs more time for reaching the asymptotic value once the agglomerates become bigger. τ_f becomes A if the initial aerosols start from monodisperse (σ_{g0}=1) shape. Through these processes, the newly developed equations will play a role in estimating the time for reaching the asymptotic value.

6. Implication to Nanoparticle Synthesis

The synthesized PPS is usually larger than 2 nm in many industrial applications. For instance, TiO_2 is synthesized via flame, and the primary particle size is roughly 20 nm [31], and the primary particle size of anatase TiO_2 nanoparticles synthesized via chemical vapor deposition (CVD) is between 12 and 23 nm [32]. Prior models used 2 nm for PPS of 2 nm [19,22]. Although the influence of d_p for a small D_f (e.g. 2) is negligible, τ_f increases exponentially as d_p increases when D_f is 3 (Fig. 4). Based upon Eq. (17), 20 nm primary

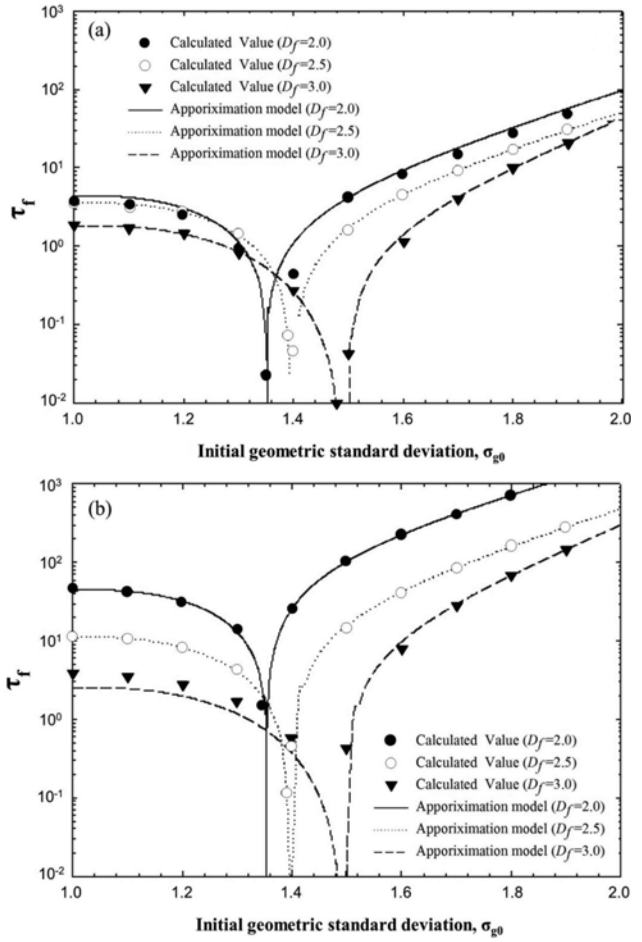

Fig. 5. D_f and σ_{g0} effects on the SPT lag: (a) d_p=2 nm; (b) d_p=20 nm.

particles take more time than 2 nm primary particles for reaching a self-preserving distribution. This is modifiable by the new formula which provides a more accurate estimation in terms of the effects of important parameters.

CONCLUSION

We investigated the influences of initial GSD and PPS on the change in SPT lag and GSD of fractal agglomerates with regards to the free molecular regime. The moment method presents very similar results to those of the analytical solution. On the other hand, the values obtained by sectional methods were not sufficiently close to the asymptotic values because of the assumptions on the size distribution applied to these models.

The reliance between σ_{g0} and τ_f had an exponential relationship with the PPS, initial GSD, and MFD. The asymptotic GSD had nothing to do with PPS. The influence of PPS to the SPT lag was insignificant in the case of small the MFD (D_f=2.0). SPT lag is reduced as the initial GSD approaches the asymptotic value. A statistical formula was developed with high R^2 values (>0.99) for SPT lag on initial GSD, PPS, and MFD of agglomerates. The developed formulae in this study will be used for a convenient method to evaluate the SPT lag of fractal agglomerates.

ACKNOWLEDGEMENTS

This work was supported by the Basic Science Research Program through the National Research Foundation of Korea (NRF) funded by the Ministry of Science and ICT (NRF-2017R1C1B1008811).

SUPPORTING INFORMATION

Additional information as noted in the text. This information is available via the Internet at http://www.springer.com/chemistry/journal/11814.

REFERENCES

1. S. E. Pratsinis, *Prog. Energy Combust. Sci.*, **24**, 197 (1998).
2. W. J. Stark and S. E. Pratsinis, *Powder Technol.*, **126**, 103 (2002).
3. S. K. Friedlander and D. Y. H. Pui, *J. Nanopart. Res.*, **6**, 313 (2004).
4. S. Wunder, F. Polzer, Y. Lu, Y. Mei and M. Ballauff, *J. Phys. Chem. C*, **114**, 8814 (2010).
5. A. Schmidt-Ott, *Appl. Phys. Lett.*, **52**, 954 (1988).
6. T. Matsoukas and S. K. Friedlander, *J. Colloid Interface Sci.*, **146**, 495 (1991).
7. M. K. Akhtar, Y. Xiong and S. E. Pratsinis, *AIChE J.*, **37**, 1561 (1991).
8. Y.-W. Oh, K.-J. Jeon, A.-I. Jung and Y.-W. Jung, *Aerosol Sci. Technol.*, **36**, 573 (2002).
9. M. K. Akhtar, G. G. Lipscomb and S. E. Pratsinis, *Aerosol Sci. Technol.*, **21**, 83 (1994).
10. R. D. Mountain, G. W. Mulholland and H. Baum, *J. Colloid Interface Sci.*, **114**, 67 (1986).
11. P. Meakin, P. Ramanlal, L. M. Sander and R. C. Ball, *Phys. Rev. A*, **34**, 5091 (1986).
12. D. W. Schaefer, *MRS Bull.*, **13**, 22 (1988).
13. K. T. Whitby, *Lumped mode aerosol growth model*, Particle Technology Laboratory Publication #395, University of Minnesota, Minneapolis (1979).
14. K. W. Lee and H. Chen, *Aerosol Sci. Technol.*, **3**, 327 (1984).
15. M. Frenklach and S. J. Harris, *J. Colloid Interface Sci.*, **118**, 252 (1987).
16. F. Gelbard and J. H. Seinfeld, *J. Colloid Interface Sci.*, **78**, 485 (1980).
17. J. D. Landgrebe and S. E. Pratsinis, *J. Colloid Interface Sci.*, **139**, 63 (1990).
18. M. K. Wu and S. K. Friedlander, *J. Aerosol Sci.*, **24**, 273 (1993).
19. S. Vemury, K. A. Kusters and S. E. Pratsinis, *J. Colloid Interface Sci.*, **165**, 53 (1994).
20. S. Vemury and S. E. Pratsinis, *J. Aerosol Sci.*, **26**, 175 (1995).
21. K. W. Lee, L. A. Curtis and H. Chen, *Aerosol Sci. Technol.*, **12**, 457 (1990).
22. S. H. Park and K. W. Lee, *J. Colloid Interface Sci.*, **246**, 85 (2002).
23. C.-Y. Wu and P. Biswas, *Aerosol Sci. Technol.*, **29**, 359 (1998).
24. G. D. Ulrich and N. S. Subramanian, *Combust. Sci. Technol.*, **17**, 119 (1977).
25. S. K. Friedlander, *Smoke, dust and haze: fundamentals of aerosol dynamics*, Oxford Univ. Press, New York (2000).
26. B. B. Mandelbrot, *The Fractal Geometry of Nature*, Freeman and Co., New York (1982).
27. E. R. Whitby, P. H. McMurry, U. Shankar and F. S. Binkowski,

Modal aerosol dynamics modeling, Computer Sciences Corp., Research Triangle Park (1991).
28. M. M. R. Williams and S. K. Loyalka, *Aerosol science: Theory and practice*, Pergamon Press, Oxford (1991).
29. S. Park and K. Lee, *J. Colloid Interface Sci.*, **233**, 117 (2001).
30. S. Park, R. Xiang and K. Lee, *J. Colloid Interface Sci.*, **231**, 129 (2000).
31. P. F. Miquel, C.-H. Hung and J. L. Katz, *J. Mater. Res.*, **8**, 2404 (1993).
32. U. Backman, U. Tapper and J. K. Jokiniemi, *Synth. Met.*, **142**, 169 (2004).